The refreezing of melt ponds on Arctic sea ice

AGU PUBLICATIONS

JGR

Journal of Geophysical Research: Oceans

RESEARCH ARTICLE

10.1002/2014JC010140

The refreezing of melt ponds on Arctic sea ice

Daniela Flocco[1], Daniel L. Feltham[1], Eleanor Bailey[2], and David Schroeder[1]

[1]Centre for Polar Observation and Modelling, Department of Meteorology, University of Reading, Reading, UK, [2]C-CORE's Centre for Arctic Resource Development, St. John's, Newfoundland, Canada

Key Points:
- Salt release delays melt pond refreezing
- Pond refreezing prevents basal sea ice growth for some time
- Refreezing is increasingly important over thin ice

Correspondence to:
D. Flocco,
d.flocco@reading.ac.uk

Citation:
Flocco, D., D. L. Feltham, E. Bailey, and D. Schroeder (2015), The refreezing of melt ponds on Arctic sea ice, *J. Geophys. Res. Oceans*, *120*, 647–659, doi:10.1002/2014JC010140.

Received 9 MAY 2014
Accepted 5 JAN 2015
Accepted article online 8 JAN 2015
Published online 5 FEB 2015

Abstract The presence of melt ponds on the surface of Arctic sea ice significantly reduces its albedo, inducing a positive feedback leading to sea ice thinning. While the role of melt ponds in enhancing the summer melt of sea ice is well known, their impact on suppressing winter freezing of sea ice has, hitherto, received less attention. Melt ponds freeze by forming an ice lid at the upper surface, which insulates them from the atmosphere and traps pond water between the underlying sea ice and the ice lid. The pond water is a store of latent heat, which is released during refreezing. Until a pond freezes completely, there can be minimal ice growth at the base of the underlying sea ice. In this work, we present a model of the refreezing of a melt pond that includes the heat and salt balances in the ice lid, trapped pond, and underlying sea ice. The model uses a two-stream radiation model to account for radiative scattering at phase boundaries. Simulations and related sensitivity studies suggest that trapped pond water may survive for over a month. We focus on the role that pond salinity has on delaying the refreezing process and retarding basal sea ice growth. We estimate that for a typical sea ice pond coverage in autumn, excluding the impact of trapped ponds in models overestimates ice growth by up to 265 million km^3, an overestimate of 26%.

1. Introduction

Melt ponds form on Arctic sea ice from the accumulation in topographic lows of meltwater created from melting of snow and ice. They can cover almost 50% of the sea ice surface and have a strong impact on the albedo of the ice surface: melt ponds can have an albedo as low as 0.15, while the albedo of bare sea ice is as high as 0.8. This albedo difference enhances the melting of sea ice in the presence of ponds, generating a positive feedback mechanism of sea ice melt [*Perovich*, 1990; *Schröder et al.*, 2014].

A given volume of surface meltwater will produce shallow, large-area ponds on relatively flat first-year ice (FYI) and deeper, smaller-area ponds on relatively rough multiyear (MYI) or ridged sea ice. While the albedo of ponded sea ice does decrease with pond depth [*Taylor and Feltham*, 2004], the dominant impact on the area-averaged albedo comes from increasing pond area [*Scott and Feltham*, 2010]. In the last decade, the relative fraction of FYI has increased in the Arctic, with a 40% reduction in MYI volume over the period 2005–2008 [*Kwok et al.*, 2009], and therefore, study of the physics of melt ponds and their proper representation in GCMs has become increasingly important.

Previous modeling studies of melt ponds have focused on their formation and summertime evolution [*Taylor and Feltham*, 2004; *Flocco and Feltham*, 2007; *Flocco et al.*, 2010, 2012; *Lüthje et al.*, 2006; *Skyllingstad*, 2009]. In autumn, the ponds refreeze at their upper surface to form an ice lid, which insulates them from the atmosphere and traps pond water between the sea ice and the ice lid. The lid's albedo quickly increases to the value of sea ice albedo insulating the pond both thermodynamically and optically. The pond water is a store of latent heat that is released during refreezing, and until the pond freezes completely there can be minimal ice growth at the base of the sea ice. A first attempt at modeling the refreezing of melt ponds was described in *Taylor and Feltham* [2004], although this ignored the role of pond salinity. A simpler version of this approach, essentially treating the ice lid growth as a classic Stefan phase change problem, was incorporated into a climate sea ice model by *Flocco et al.* [2010, 2012]. Based on these works, *Hunke et al.* [2010] developed another

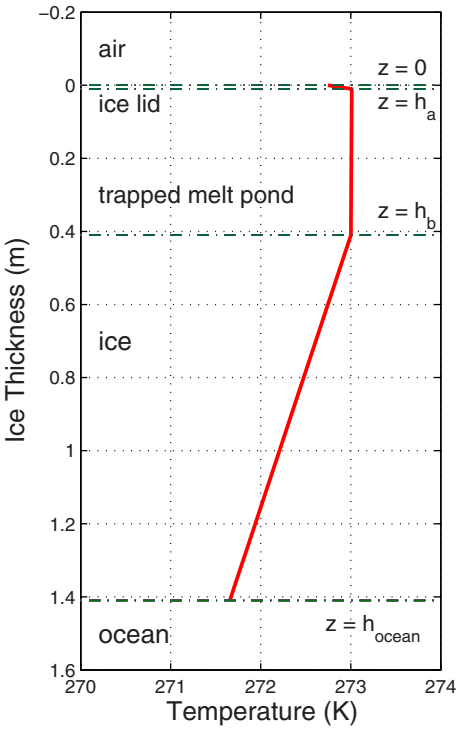

Figure 1. Definition sketch showing the initial configuration of ice lid, trapped pond, sea ice, and ocean. The red line is the initial temperature profile in the reference state.

melt pond routine based on similar principles. The model presented by *Flocco et al.* [2010, 2012] distinguishes between active (no ice lid) and nonactive ponds that are covered by an ice lid.

A similar problem to the refreezing of melt pond was studied by *Bailey et al.* [2010] who developed a one-dimensional consolidation model to investigate the freezing process between two rafted ice sheets separated by a thin liquid layer. Since the liquid layer was narrow, they assumed the temperature would remain uniform. They accounted for the influence of salinity on the freezing process by assuming a fraction of salt originally contained in the seawater was expelled into the liquid layer. *Bogorodskiy and Marchenko* [2014] recently developed a similar model to describe the refreezing of melt ponds in autumn-winter, where they also made the assumption that the temperature in the liquid region (i.e., the pond in this case) remained uniform based on the fact that there was sufficient convective mixing. They, however, did not describe the heat and salt distribution in the ice layers.

In this paper, we present a one-dimensional model that was developed based on similar principle to that of *Bailey et al.* [2010] to investigate the refreezing of melt ponds in the Arctic. The model we have implemented considers the heat and salt balances in the ice lid, trapped pond, and underlying sea ice. We include a two-stream radiation model to account for radiative scattering at phase boundaries and examine the role of pond salinity in controlling the refreezing process.

Our paper is structured as follows: in section 2, we describe the model of freezing melt ponds; in section 3, we investigate results from our model's simulation of the refreezing process for a typical, reference case and present results from sensitivity studies investigating the role of ambient conditions and treatment of pond salinity. We summarize our main findings and speculate on their implication for the Arctic sea ice mass budget in section 4.

2. A Model of Sea Ice Growth

We have developed a one-dimensional model of the refreezing of a melt pond on sea ice. Figure 1 depicts the initial configuration of components: we initialize with a thin ice lid that has formed on the pond surface, separating the trapped pond from the air above; the trapped pond sits above a sea ice layer floating upon the ocean. The initial conditions for this study are based on a field study by *Marchenko et al.* [2009]. The focus of this study is purely on the refreezing of the pond, and we do not attempt an annual simulation that would introduce complicating factors not pertinent to our study. The following subsections describe the heat and salt balance and radiative equations to be solved in the ice and trapped pond and the necessary boundary conditions.

2.1. Heat and Salt Balances in the Sea Ice and Ice Lid

The sea ice and ice lid comprise a solid pure ice phase embedded with brine inclusions and are therefore mushy layers [*Feltham et al.*, 2006]. The heat and salt balances within the sea ice and ice lid are linked together via the constraint of thermodynamic equilibrium, so that the temperature is determined from a nonlinear equation that accounts for internal phase change. In the absence of brine flow, which we shall assume (later shown to be justified) that the heat balance equation is equivalent to that from previous models of sea ice [e.g., *Maykut and Untersteiner*, 1971] and is

$$c_{eff}\frac{\partial T}{\partial t}=\frac{\partial}{\partial z}\left(k_{eff}\frac{\partial T}{\partial z}\right)+\frac{\partial F_{net}(z)}{\partial z}, \tag{1}$$

where F_{net} is the net flux and c_{eff} is the effective volumetric heat capacity defined by

$$c_{eff}=c_i+\frac{T_L(S_{bulk})-T_L(0)}{\theta^2}L, \tag{2}$$

where $c_i = 1.883 \times 10^6$ J/(m^3 K) is the specific volumetric heat capacity of sea ice, $T_L(S)$ denotes the liquidus (freezing) temperature of water with salinity S (e.g., $T_L(0) = 0°$C), $\theta = T - T_L(0)$, and $L = 3.014 \times 10^8$ J m^{-3} is the volumetric latent heat of fusion of pure ice [*Bitz and Lipscomb*, 1999; *Feltham et al*., 2006; *Bailey et al*., 2010]. The effective thermal conductivity of sea ice is given by

$$k_{eff}=k_{bi}-(k_{bi}-k_b)\frac{T_L(S_{bulk})-T_L(0)}{\theta}, \tag{3}$$

where k_{bi} and k_b are, respectively, the conductivities of bubbly ice and brine, defined as

$$k_{bi}=\frac{2k_i+k_a-2V_a(k_i-k_a)}{2k_i+k_a+2V_a(k_i-k_a)}k_i, \tag{4}$$

and

$$k_b=\ 0.4184(1.25+0.030\theta+0.00014\theta^2), \tag{5}$$

where $k_i = 1.16$ (1.91 $- 8.66 \times 10^{-3}\ \theta + 2.97 \times 10^{-5}\ \theta^2$) W (m K)$^{-1}$ is the conductivity of pure ice [*Schwerdtfeger*, 1963; *Sakazume and Seki*, 1978], $k_a = 0.03$ W (m K)$^{-1}$ is the conductivity of air [*Weeks and Ackley*, 1986], and we have assumed a constant $V_a = 0.025$ as the fractional volume of air in sea ice [*Timco and Frederking*, 1996].

At the air-ice-lid interface or air-sea-ice interface in the absence of a melt pond ($z = 0$), the surface temperature boundary condition is given by the surface energy balance, which is

$$F_{LW}-\varepsilon\sigma T^4+F_{SW}(1-\alpha)(1-I_0)-F_{sens}-F_{lat}=k_{eff}\frac{\partial T}{\partial z}, \tag{6}$$

where F_{LW} and F_{SW} are the downward fluxes of longwave and shortwave radiation, $\varepsilon = 0.99$ is the emissivity of sea ice, $\sigma = 5.67 \times 10^{-8}$ J (K^4 m^2 s)$^{-1}$ is the Stefan-Boltzmann constant, α is the albedo of sea ice and the lid which are assumed to be identical, I_0 is the fraction of solar radiation penetrating the surface layer (considered to be of negligible thickness), and $F_{sen}T\ =\ T_L(S_{ocean})_s$ and F_{lat} are the sensible and latent heat fluxes [*Ebert and Curry*, 1993; *Maykut and Untersteiner*, 1971; *Taylor and Feltham*, 2004; *Bailey et al*., 2010].

Thermodynamic equilibrium at the sea-ice-ocean and melt-pond-ice interfaces determines further boundary conditions on the temperature. The boundary condition at the bottom of the ice ($z = h_{ocean}$) is

$$T=T_L(S_{ocean}), \tag{7}$$

where S_{ocean} is the ocean salinity at the ice-ocean interface, and the boundary conditions at the bottom of the ice lid ($z = h_a$) and the top of the bottom sea ice layer ($z = h_b$) are

$$T_l=T_p=T_L(S), \tag{8}$$

where S is the pond salinity at the interface, discussed below.

Any imbalance of heat flux at the sea ice-ocean interface and ice lid-pond interfaces will drive phase change, described by the Stefan condition. At the sea ice-ocean interface ($z = h_{ocean}$),

$$\frac{\rho_{brine}}{\rho_{ice}}L\phi\frac{\partial h_{ocean}}{\partial t}=k_{eff}\frac{\partial T}{\partial z}+F_{ocean}, \tag{9}$$

where the density ratio of seawater to sea ice $\frac{\rho_{ocean}}{\rho_{ice}}=1.09$ accounts for the expansion of sea ice on freezing, ϕ is the solid fraction of sea ice at the ice-ocean interface, and F_{ocean} is the heat flux at the sea ice bottom [*Bitz and Lipscomb*, 1999; *Feltham et al*., 2006; *Bailey et al*., 2010]. At the ice-lid-pond ($z = h_a$) and sea-ice-pond ($z = h_b$) interfaces, the Stefan boundary condition is

$$\frac{\rho_{brine}}{\rho_{ice}} L\phi \frac{\partial h}{\partial t} = k_{eff} \frac{\partial T_{ice}}{\partial z} - k_p \frac{\partial T_{pond}}{\partial z}, \tag{10}$$

where k_p is the thermal conductivity of the pond water. The solid fraction at the interface of the sea ice and lid with the ocean or liquid is given by

$$\varphi = 1 - \frac{S_{bulk}}{S_{\text{interface}}}, \tag{11}$$

where S_{bulk} is the bulk salinity of the sea ice or lid and $S_{\text{interface}}$ is the salinity in the liquid at the interface. S_{bulk} will vary throughout the interface region [*Feltham et al*., 2006; *Notz and Worster*, 2008]. We have introduced a new expression to calculate the amount of salt that gets trapped into the ice lid during the freezing of the pond: when the ice is growing the bulk salinity of the layer of ice formed in a time step is calculated using the solid fraction and trapped pond salinity at the interface to be:

$$S_{bulk} = \frac{S_{\text{interface}}}{(1-\varphi)}.$$

When the ice is dissolving the salinity of the solution produced at the interface is calculated from the brine salinity in the ice dissolved to be:

$$S_{\text{interface}} = S_{brine}(1-\varphi).$$

This approach conveys the mathematical advantage that the parameters at the interface location can be determined explicitly rather than using an implicit numerical technique and leads to little numerical error [*Feltham*, 1998]. The resolution varies from submillimeter resolution when the lid is very thin up to a centimeter resolution when the pond is refrozen.

2.2. Heat and Salt Balances in the Trapped Pond

Buoyancy forces in a melt pond exposed directly to the atmosphere cause the pond to become turbulent [*Taylor and Feltham*, 2004]. Once an ice lid forms, salt is released into the meltwater at the growing interface, which creates a source of negative buoyancy. Calculation of the Rayleigh number in the pond shows it to be supercritical, i.e., the trapped pond is turbulent, for the full geophysical range of pond salinities (1–2 psu up to about 25 psu). While turbulence ensures the core of the trapped pond is of uniform temperature and salinity, the continuous input of salt from the freezing ice lid creates a salty layer at the lid-pond interface. The heat balance in the trapped pond assumes the form of a standard heat diffusion equation, with a turbulent-enhanced thermal diffusivity, with a source of heat from absorbed solar radiation (the divergence of the net irradiance F_{net})

$$\frac{\partial T}{\partial t} = \frac{\partial}{\partial z}\left(\kappa \frac{\partial T}{\partial z}\right) + \frac{1}{c_{eff}} \frac{\partial F_{net}(z)}{\partial z}, \tag{12}$$

where we set the turbulent diffusivity to be $\kappa = 10^{-2}\ \text{m}^2\ \text{s}^{-1}$ (the calculations presented are not sensitive to variation of this value by a factor of 100). Similarly, we write the salt balance in the trapped pond as

$$\frac{\partial S}{\partial t} = \frac{\partial}{\partial z}\left(D_{turb} \frac{\partial S}{\partial z}\right), \tag{13}$$

where $D_{turb} = 10^{-2}\ \text{m}^2\ \text{s}^{-1}$ is the turbulent-enhanced diffusion coefficient of salt.

The boundary conditions on temperature at the top and the bottom of the pond are determined by the requirement that temperature is continuous (equation (8)). Conservation of salt at the upper ($z = h_a$) and lower surfaces ($z = h_b$) of the trapped pond requires

$$\phi(S - S_i)\frac{dh}{dt} = D\frac{\partial S}{\partial z}, \tag{14}$$

which balances the salt released at the freezing lid-pond and pond-sea ice interfaces with salt diffusion away from the interface. S_i is the salt incorporated directly into the ice phase (i.e., not the brine pockets) and is negligible, we take $S_i = 0$ in the following. D is the molecular diffusion coefficient of salt, taken to be $1.2 \times 10^{-11}\ \text{m}^2\ \text{s}^{-1}$).

While solution of the temperature and salinity equations inside the pond is technically straightforward, the low molecular diffusion coefficient of salt generates narrow (submillimeter) solutal boundary layers at the pond interfaces that are impractical to resolve in seasonal or climate calculations. Therefore, while we solve the temperature equation numerically, we introduce a semianalytical approximation for the salt balance,

$$S(z)=\alpha_s e^{-\frac{z-h_a}{L_a}}+\beta_s e^{\frac{z-h_b}{L_b}}+\gamma_s, \tag{15}$$

where the solutal boundary layer depths are

$$L_a=\frac{D}{dh_a/dt}, L_b=\frac{D}{dh_b/dt}. \tag{16}$$

Since $L_a, L_b \ll h_b-h_a$, the two exponential terms in the formula for pond salinity vary strongly with position across the upper and lower solutal boundary layers.

Substituting equation (15) into (14) at $z=h_a$, we obtain

$$\phi_a\left(\alpha_s+\beta_s e^{-\frac{h_a-h_b}{L_b}}+\gamma_s-S_i\right)\frac{dh_a}{dt}=-D\left(\frac{\alpha_s}{L_a}+\frac{\beta_s}{L_b}e^{-\frac{h_a-h_b}{L_b}}\right). \tag{17}$$

Since $|h_a-h_b|/L_b \gg 1$, equation (17) can be solved, using equation (16), to yield

$$\alpha_s=\frac{\gamma_s\phi_a}{1-\phi_a}. \tag{18}$$

Similarly, we derive

$$\beta_s=\frac{\gamma_s\phi_b}{1-\phi_b}, \tag{19}$$

and so our salinity profile becomes

$$S(z)=\gamma_s\left\{\frac{\phi_a}{1-\phi_a}e^{-\frac{z-h_a}{L_a}}+\frac{\phi_b}{1-\phi_b}e^{\frac{z-h_b}{L_b}}+1\right\}. \tag{20}$$

The parameter γ_s evolves with time as salt enters the pond as it freezes at its interfaces. The average pond salinity at time j, $\overline{S}^j$, is derived from conservation of salt,

$$(h_b^j-h_a^j)\overline{S}^j=\overline{S}^{j-1}(h_b^{j-1}-h_a^{j-1})+\left(\overline{S}^{j-1}-S_{lid}^{bulk}\right)\Delta h^j{}_a-\left(\overline{S}^{j-1}-S_{ice}^{bulk}\right)\Delta h^j{}_b. \tag{21}$$

We determine $\gamma_s{}^j$ from the requirement that $\int_{h_a}^{h_b} S(z)|_{t_j}dz=(h_a-h_b)\overline{S}^j$ to be

$$\gamma_s=\frac{(h_b-h_a)}{(h_b-h_a)+\frac{\phi_a L_a}{1-\phi_a}+\frac{\phi_b L_b}{1-\phi_b}}\overline{S}^j\approx\overline{S}^j, \tag{22}$$

where we have used $e^{-\frac{h_a-h_b}{L_a}}\simeq 0$ and $e^{-\frac{h_a-h_b}{L_b}}\simeq 0$ to obtain the first expression in equation (22).

It is interesting to note that if the salinity at the ice-lid-pond interface becomes high enough, then the freezing temperature can become lowered until there is no conductive heat flux through the lid to the atmosphere (i.e., the temperature gradient between the ice-atmosphere and the pond-upper ice lid disappears), at which point the lid will cease to freeze.

2.3. Radiation Balance

In sea ice models that do not treat melt ponds as a separate phase, the treatment of solar radiation absorption typically uses Beer's law in which the intensity of transmitted radiance is exponentially attenuated

$$F_{net}=I_0(1-\alpha)F_{SW}e^{-\lambda z}, \tag{23}$$

where λ is the extinction coefficient and the albedo α is prescribed [e.g., *Ebert and Curry*, 1993]. While Beer's law may be efficiently implemented, it ignores scattering from the ice bottom and is formally only applicable for infinitely thick layers. In practice, basal scattering has a small effect for ice thicker than about 2 m [*Taylor and Feltham*, 2004] but since most sea ice is thinner than this and since there are multiple scattering

interfaces when melt ponds are present, Beer's law is not appropriate for our study. Consequently, we have adopted the two-stream radiation scheme described in *Perovich* [1990] and applied by *Taylor and Feltham* [2004] to a model of melt ponds on sea ice. By resolving the irradiance into upwelling and downwelling streams, this model allows us to account for the solar radiation reflected back into the ice and pond at the lid-pond interfaces. The net flux is

$$F_{net\,i} = F_{\downarrow i} - F_{\uparrow i}, \tag{24}$$

where the downwelling $F_{\downarrow i}$ and upwelling irradiance $F_{\uparrow i}$ are determined from

$$\begin{cases} \dfrac{\partial F_{\downarrow i}}{\partial z_i} = -(k_{ai} + r_{si})F_{\downarrow i} + r_{si}F_{\uparrow i} \\ \dfrac{\partial F_{\uparrow i}}{\partial z_i} = (k_{ai} + r_{si})F_{\uparrow i} + r_{si}F_{\downarrow i} \end{cases}, \tag{25}$$

where k_{ai} (m^{-1}) and r_{si} (m^{-1}) are, respectively, the absorption and scattering coefficients, and the suffix i denotes the component: $i = 0$, 1, 2 being, respectively, the ice lid, melt pond, and sea ice below the pond. The boundary conditions on the irradiances are

$$F_{\downarrow 0} = (1 - R_0)F_{SW} + R_0 F_{\uparrow 0}, \tag{26}$$

at the ice-air interface and

$$F_{\uparrow 2} = 0, \tag{27}$$

at the ice-ocean interface, and continuity of upwelling and downwelling fluxes at the lid-pond and pond-ice interfaces. R_0 is the Fresnel reflection coefficient at the air-ice interface [*Perovich*, 1990]. The albedo is calculated from

$$\alpha = R_0 + \frac{(1 - R_0)F_{\uparrow 0}(z = 0)}{F_{SW}}. \tag{28}$$

The solutions for the irradiances, and further details of the calculation, are given in *Taylor and Feltham* [2004].

3. Numerical Simulation Results

Our model is forced with atmospheric and oceanic forcing data, which comprises six-hourly, 2 m air temperature, and daily downward shortwave and longwave radiation fluxes from ERA-Interim, a constant wind speed of 6 m s^{-1}, constant atmospheric pressure of 1013 mbar, zero precipitation, and 2 W m^{-2} ocean heat flux into the base of the sea ice. The air temperature, downward shortwave and longwave radiation have been interpolated using a Gaussian distribution and are depicted in Figure 2 at three different locations: 80°N, 210°E (our reference case); 75°N, 210°E; and 89°N, 210°E. Note that since the longwave radiation is affected by the cloud cover, there is no clear north-south trend unlike the air temperature and the shortwave radiation.

Open pond salinities are in the range 1–30 psu, but more commonly values lower than 5 psu are observed [*Perovich et al.*, 2009], with pond temperatures around −0.5°C (calculated using the liquidus curve). The model simulations are run from the 31 August (Julian day 243) for 60 days. In the following subsections, we present model simulations for a typical reference case, and examine the importance of the treatment of salinity in the trapped pond on the rate of pond refreezing. We then consider a number of sensitivity studies starting from the reference state, varying the latitude and longitude of the atmospheric forcing, initial sea ice thickness and salinity, pond depth, and ocean heat fluxes.

3.1. Reference Run (80°N, 210°E)

The initial configuration of components, and initial temperature profile, for our reference run is depicted in Figure 1. The refreezing melt pond is 0.4 m deep covered by a 1 cm layer of ice and the underlying sea ice layer is 1 m thick. The salinity of the lid is set at 11 psu and the salinity of the sea ice below the pond is 33 psu, while the salinity in the interior of the pond (γ at $t = 0$) is set to be 1.8 psu and the initial salinity at the interfaces between the pond and the ice is dependent on the solid fraction and the temperature at the

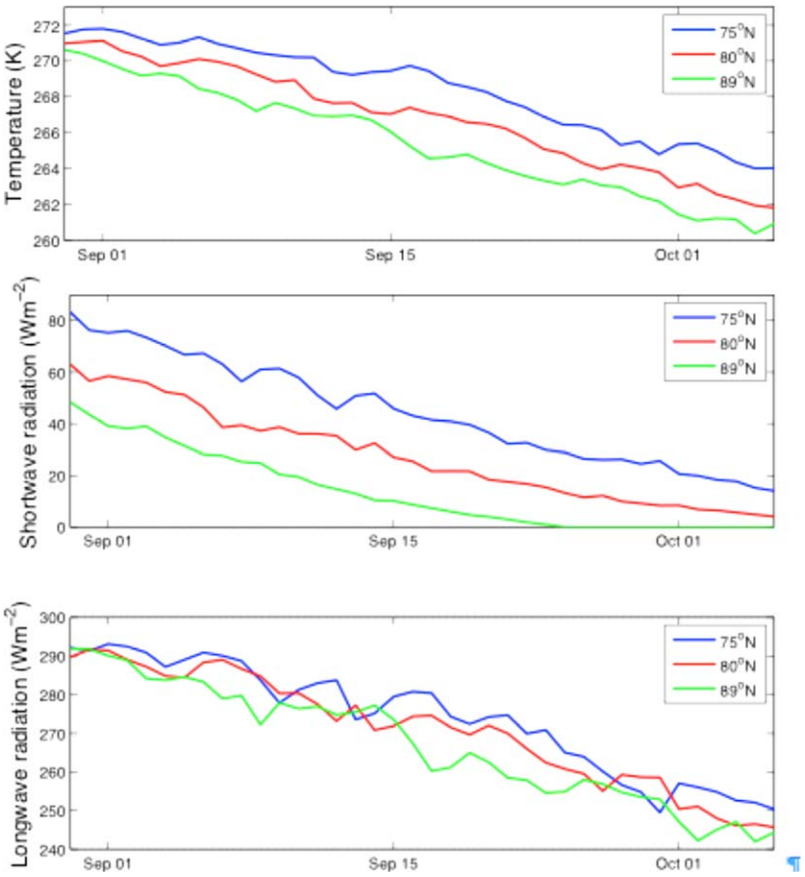

Figure 2. (a) Air temperature at 2 m; (b) shortwave radiation; and (c) longwave radiation at 80°N, 210°E (our reference case); 75°N, 210°E; and 89°N, 210°E.

interface between the pond and the ice. The salinity at the interface between the ice and the ocean is taken to be 25 psu, a value typical of summer conditions where meltwater freshens the upper part of the mixed layer [*Notz et al.*, 2003]. The heat flux from the ocean and the atmospheric and oceanic forcing have been described above; our reference run uses data at 80°N, 210°E.

At each time step, the brine salinity of the lid and the ice under the pond is calculated by using a formulation proposed by *Assur* [1958] for seawater that inverts the liquidus curve.

Figure 3 shows the calculated evolution of the temperature profile, from which one can also discern the phase boundaries as discontinuities in the temperature derivative. The latent heat released from freezing of the trapped pond prevents basal ice growth until the pond has completely frozen. The melt pond freezes in 33 days but basal growth does not start for further 18 days after the pond has completely frozen. At that point, the temperature profile in the ice becomes almost linear and seawater starts freezing at the ice base and the ice thickens by 0.02 m in the subsequent 9 days. The comparison with an equivalent sea ice thickness of 1 m with no trapped pond gives us a significant result: from our runs we observe that the ice starts growing from the beginning of the simulation to reach an ice thickness of 1.24 m after 60 days, with a total ice growth of 0.24 m. Thus, while highly idealized because we have neglected the effect of snow, lateral redistribution of ice and other processes, our simulations indicate that the presence of a trapped pond induces a significant reduction in ice growth.

The pond freezes relatively quickly at the beginning of the simulation but then slows due to the increasing salinity at the lid-pond interface that lowers the freezing temperature there (Figure 4). In the middle plot, the position of the freezing front at the top of the trapped pond can be observed. Figure 4 also shows the (less rapid) ablation, due to dissolution [*Feltham and Worster*, 2000], at the base of the trapped pond and the corresponding rise in the pond salinity at the interfaces and in the middle of the pond. The salinity at

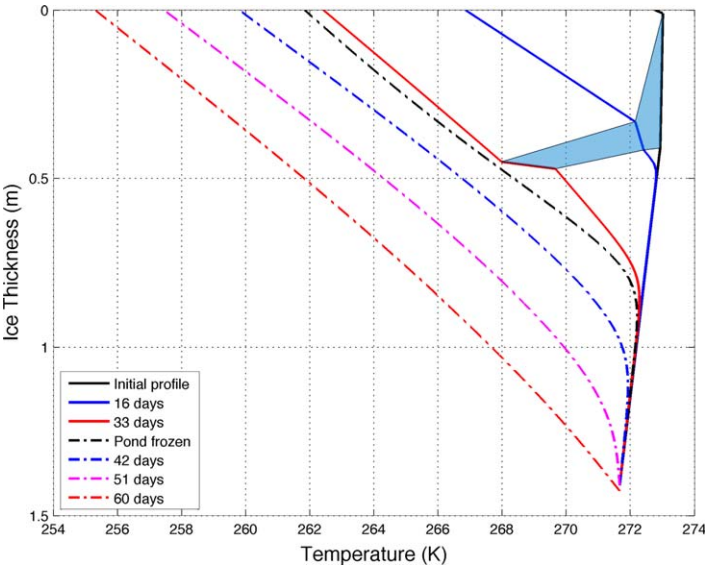

Figure 3. Ice-pond temperature profile at 80°N, 210°E. The region colored blue is the trapped melt pond.

the pond's interfaces increases more quickly than in the pond. The average salinity of the pond reaches a maximum of 72.4 psu with 91.9 psu in the solutal boundary layer. The salinity of the lid reaches values of 44.8 psu while due to sea ice dissolution at the pond's bottom the ice reaches a salinity value of 7.9 psu. Note there is no drainage of salty pond water through the ice into the ocean below in our simulation. Calculation of the porous medium Rayleigh number in the ice below the trapped pond reveals that gravity drainage does not occur during our simulation with a critical Rayleigh number of 10 [*Notz and Worster*, 2008]. Gravity drainage occurs from Day 33 of the simulation but the calculated salt flux, following *Wells et al*. [2011], is in the order of 10^{-3}–10^{-2} psu d^{-1} and can therefore be neglected for our purposes. The small amount of drainage is mostly due to the low ice permeability during the refreezing time: it ice starts at 10^{-10} m^2 and goes down to 10^{-12} m^2.

The condition for considering the refreezing process concluded is not a cutoff value of the pond depth, as was implemented in *Bailey et al*. [2010] but is instead linked to an interesting behavior of the pond. Freezing at the top of the trapped pond and ablation at its base results in a downward migration of the trapped pond. This is similar to the behavior observed in *Bailey et al*. [2010] and *Bogorodskiy and Marchenko* [2014].

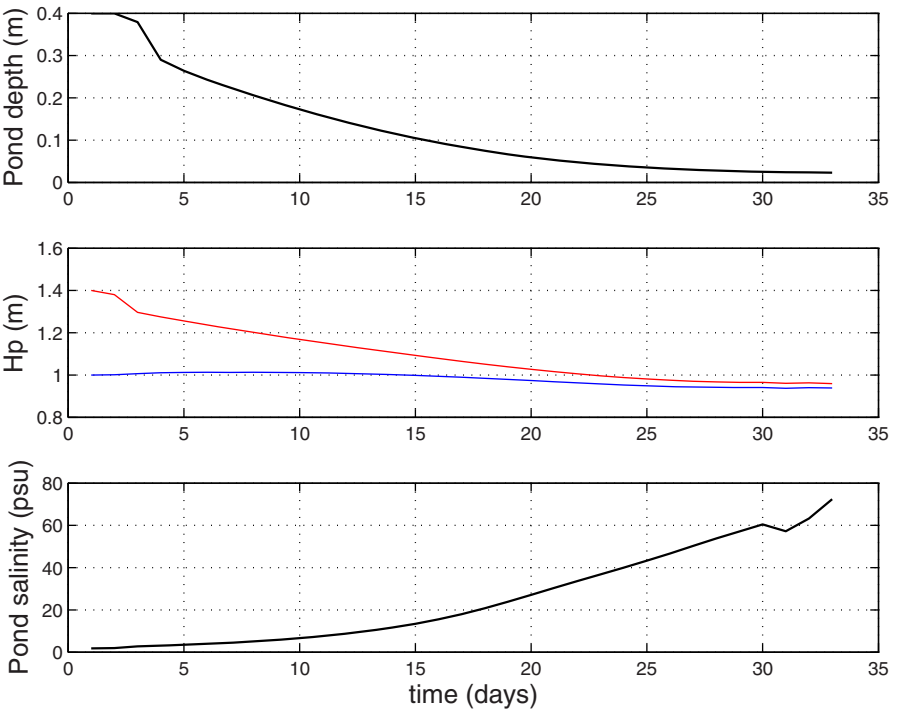

Figure 4. (a) Pond depth evolution, (b) position of freezing fronts, and (c) salinity evolution at 80°N 210°E (standard run).

Table 1. Freezing Time of a Trapped Melt Pond With Different Initial Salinity Profiles

	Final Trapped Pond Salinity (psu)		Number of Days Until the Pond Is Frozen		Starting Day for Ice Growth	
Initial Trapped Pond Salinity (psu)	Uniform Salinity Model	Salinity Boundary Layer Included	Uniform Salinity Model	Salinity Boundary Layer Included	Uniform Salinity Model	Salinity Boundary Layer Included
1.8	45.0	72.4 (interior) 91.9 (lid)	19	33	41	51
5.0	92.4	132.1 (interior) 149.5 (lid)	41	46	47	47
10.0	122.9	152.4 (interior) 176.1 (lid)	61	Not frozen (8 cm at 60 days)	61	
29.0	144.8	154.8 (interior) 166.8 (lid)	Not frozen (9 cm at 60 days)	Not frozen (17 cm at 60 days)		

The freezing rate initially exceeds the basal ablation rate and the trapped pond becomes increasingly salty until the freezing rate and the ablation rate are equal.

At this point, the salinity of the trapped pond approaches the brine salinity in the ice lid and the model is effectively treating the trapped pond as a brine pocket of negligible thickness but infinite horizontal extent. This is an artifact of the model being one-dimensional, as in reality vertical and horizontal crystals growth would occur and eliminate the pond, leaving brine pockets. From this consideration, we implemented the following condition for termination of the refreezing process: that refreezing is concluded at the point at which the salinity of the solutal boundary layer exceeds the maximum brine salinity of the lid.

3.1.1. Treatment of Pond Salinity

Since the salinity at the lid-pond interface determines the freezing temperature, we decided to investigate the influence of using a uniform salinity to represent a well-mixed trapped pond. We considered initial uniform salinities of 1.8, 5, and 10 psu and then we run a series of experiments with the same values for the internal salinity in the pond but increased salinity at the ice-pond interfaces. The ice lid, ice below the pond, atmospheric and ocean forcing are as described for our reference run above. The results of these simulations are summarized in Table 1. Our results are in agreement with a previous modeling study where it was found that during melt pond freezing the meltwater salinity can reach up to 100 psu at pond depth less than 1 cm [*Bogorodskiy et al*., 2006].

When running the model using a uniform salinity profile of 1.8 psu the pond freezes in 19 days and reaches a maximum salinity of 45.0 psu with no basal growth for 39 days, while in the reference run (which includes saltier boundary layers), the pond freezes in 33 days but basal growth only starts after 53 days. The difference in sea ice growth is 0.07 m compared with the reference run where solutal boundary layers are included at both pond-sea ice interfaces.

We find that by starting at an initial uniform salinity of 5 psu the pond freezes in 41 days with a maximum salinity of 92.4 psu with basal growth starting at Day 44. When the solutal boundary layer is included, where the salinity reaches a maximum of 149.5 psu at the boundary and 132.1 psu in the interior and it takes 43 days for the pond to refreeze completely with basal growth starting at Day 44.

A different situation is found with a starting salinity of 10 psu: the number of freezing days increases to 61 without a solutal boundary layer leaving no time for sea ice growth in our simulations. In the solutal boundary layer case, a pond of 0.08 m remains after 60 days of simulation with a salinity of 152.4 in the interior of the pond and 176.1 at the boundary.

One last case considered uses a starting salinity of 29 psu, a typical salinity of ponds found in fieldwork experiments where the ponds have been flooded with seawater (Hotrax project) [*Perovich et al*., 2009]. With such a high starting salinity the pond does not completely freeze in any case and leaves a liquid gap in the ice of 0.09 and 0.17 m, respectively, for the cases without and with boundary layer with salinities lower than the ice brine salinity but too high for the pond to freeze. Cases of salinities can occur when ponds are directly flooded with seawater. We acknowledge that this model would be inadequate to represent ponds which have holes at their bottom. Our model is an idealized one and treats the cases of refreezing trapped pond with no direct contact with ocean water. These cases relate more closely to the process of under-ice melt ponds. Work on these is limited but we would suggest the most significant work to date is by *Martin and Kauffman* [1974].

Table 2. Summary of Sensitivity Study Results

	Basal Ice Growth After 60 Days (m)	Number of Days Until the Pond Is Frozen	Number of Days With No Ice Growth	Salinity at Pond Interior (psu)
Reference run (80°N, 210°E)	0.02	33	51	72
75°N, 210°E	0.00	38	55	94
89°N, 210°E	0.04	29	47	87
80°N, 280°E (cold temperature)	0.15	17	37	79
Sea ice thickness is 0.5 m	0.20	29	30	82
Sea ice thickness is 1.5 m	0.00	35	>60	93
Pond depth is 0.2 m	0.07	7	43	32
Pond depth is 0.6 m	None (min pond depth = 0.03 m)	Not frozen after 76 days	During the full simulation time	104
Ocean salinity is 8 psu	0.00	32	>60	59
Ocean salinity is 33 psu	0.05	32	44	93
Ocean heat flux is 10 W m^{-2}	0.00	34	56	90

3.2. Sensitivity Study

In this section, we consider the fate of trapped melt ponds at different locations, and explore the impact of initial ice thickness and pond depth on the refreezing process. All simulations are for 60 days. Our results are summarized in Table 2.

3.2.1. Varying Location

Along a line of constant longitude (210°E), we explore the impact on trapped pond refreezing of atmospheric forcing data (air temperature, shortwave and longwave radiation) at latitudes of 75°N, 80°N (reference case), and 89°N.

At high latitudes (89°N), the pond freezes in 29 days, with a basal growth of 0.03 m and a final thickness of 1.44 m. The opposite happens at low latitude (75°N), where the pond freezes in 38 days and reaches a maximum salinity of 88.7 psu. In this case, the brine salinity value is exceeded at Day 50 and this condition determines the change of regime in the pond's behavior. The minimum pond thickness reached is 0.03 m therefore no basal growth occurs.

Keeping the same latitude as our reference run (80°N), we choose a colder location at 80°N, 280°E. The air temperature is colder on average by 5 K (see Figure 2a) and the pond freezes in 17 days compared to 33 days in the reference run. Once the pond has frozen completely, the cold air ultimately allows for more ice growth; however, the lower surface temperature implies that a greater quantity of sensible heat must be extracted from the ice before basal growth can commence and the sea ice grows by 0.15 m at the end of the run (Figure 5).

3.2.2. Varying Initial Sea Ice Thickness and Pond Depth

Decreasing the ice thickness below the trapped pond (from 1 to 0.5 m) has an impact on both the time required for the trapped pond to freeze (29 versus 33 days) and the time for the ice growth to start after the pond has frozen (it starts after 37 days rather than 51), which causes an remarkable increase in the total amount of ice growth. This overall increase in the ice thickness is because heat can be transferred more efficiently through a thinner ice slab; the total sea ice growth was 0.20 m by the end of the simulation time. On the contrary, when we run the model with a sea ice thickness of 1.5 m, there is no major difference during the time of simulation: after 60 days though, basal growth has not started yet.

Decreasing the initial pond depth from the reference case (0.4 m) to 0.2 m results in the pond refreezing in 7 days compared to 33 days, and subsequent ice growth is reasonably enhanced (0.07 m) since ice can grow for longer.

If the initial pond depth is increased to 0.6 m, the pond does not freeze completely during the simulation period, leaving still 3 cm of pond water to freeze after 60 days of simulation with complete absence of basal growth. This happens because the pond becomes rather salty and the freezing rate at the lid-pond interface is increasingly slow.

Including the new parameterization to retain salt in the sea ice has the effect of increasing the time gap between the days when the pond freezes and basal growth starts; in fact, the effect is relatively small in the

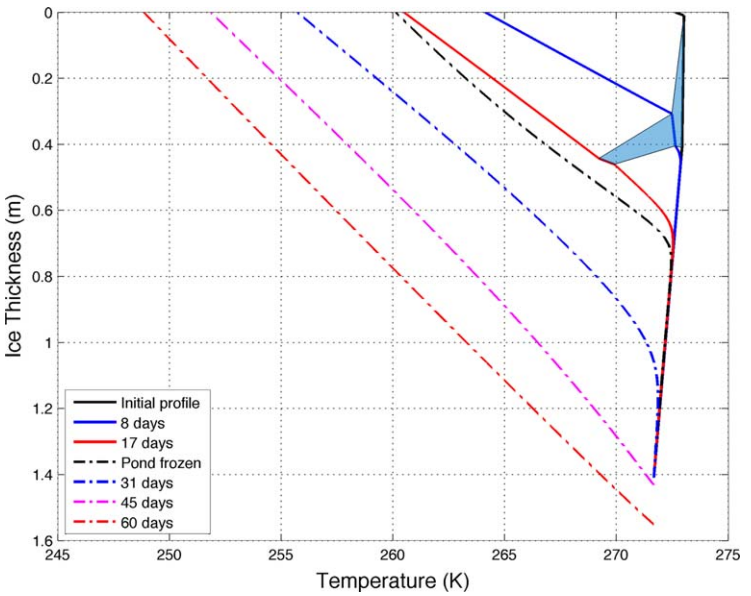

Figure 5. Ice-pond temperature profile at 80°N, 280°E. The region colored blue is the trapped melt pond.

number of freezing days when running the model with or without the enhanced salinity treatment, but compared to the standard run, the sea ice growth decreases from 7 to 2 cm during the time of simulation.

The salinity of the ocean is another variable that can present a broad range of values in correspondence with a melt pond. Seawater salinities under ponds are typically rather low since the water below the pond is a mixture of the relatively fresh ice meltwater and seawater [*Notz et al*., 2003]. In our sensitivity studies, we have used values between 8 and 33 psu. A low salinity has the effect of delaying the sea ice growth process because the ice is warmer at the ocean interface and therefore no days are available in our simulation for ice growth, while increasing the seawater salinity to 33 psu slightly leaves unaltered the number of days required for freezing but enhances the amount of sea ice growth: the pond refreezes in 33 days; however, basal ice growth starts after 44 days producing an ice growth of 5 cm. The reason for the shorter time to start basal growth is due to the fact that the since ice is initially colder at the ocean interface less heat must be extracted. In fact, the ice is initially warmer below the trapped pond because its lower boundary is kept at the freezing temperature of the ocean beneath the ice, which, being fresher, is also warmer.

A variable that is rather difficult to assess with the current data available is the ocean heat flux into the sea ice. In our reference run, we used a value of 2 W m^{-2}, which we increased to 10 W m^{-2} in our sensitivity analysis. This is considered a typical value for the end of summer [*Perovich et al*., 2009]: high heat fluxes values can be observed in autumn as it may take long for the heat stored in the summer to be released by the ocean. Results from this analysis showed that the pond refreezing time is affected by changes in the oceanic heat flux (34 days to refreeze the pond) and the number of days where basal ice growth increases even further (after 56 days).

4. Conclusion

In this work, we have shown the importance of refreezing melt ponds on sea ice growth in the autumn and early winter. The latent heat released as the trapped melt pond freezes prevents basal ice growth during this period. Furthermore, the salinity of the pond increases while ice is forming at the top of the pond causing further delay in the pond freezing and altering the salinity and temperature profiles once the pond is frozen. This result is clear when we compare the amount of sea ice growth that would take place in 60 days for a solid slab of ice with the case of a trapped pond: the ice growth is 22 cm greater when no pond is present.

We have implemented a double stream radiation scheme to account for the presence of the pond and to better describe the optical properties of the lid-pond-sea ice system.

Our new treatment of the salinity profile in the pond shows the importance of considering the salt balance and the inclusion of the parameterization of solutal boundary layer in the pond, which acts to noticeably delay the pond's refreezing when compared to the assumption of a homogeneous salinity throughout. The increased salinity of the trapped pond reduces its freezing temperature causing melt pond freezing to come to a halt if the trapped pond's salinity reaches high. A behavior found in our simulations is that the pond migrates toward the bottom of the ice and freezes completely when the balance between the freezing and ablation rates at the top and bottom interfaces of the pond is positive (freezing rate exceeds basal ablation rate).

Refreezing of ponds is a complex process: we have found that small changes in the ice thickness below the pond, ocean heat flux, and salinity of the pond cause significant effects on the sea ice growth. Even though the difference in ice growth values is rather small compared to the entire growth season, they account for a high percentage of the total possible ice growth in the time of simulation. Even with small changes in basal growth, the internal salinity profile of sea ice is often affected and, in particular, when the pond reaches very high salinities its behavior becomes analogous to a migrating brine pocket in an ice matrix.

In light of the importance of the salt balance to the refreezing process, we recommend that more measurements of sea ice salinity, pond salinity, and ocean salinity are gathered in locations where melt ponds are refreezing to force and validate our models such as ours.

Including a snow layer would delay the basal ice growth with or without a trapped pond due to its low thermal conductivity which retards heat loss in the atmosphere. This would increase the time required for trapped ponds to refreeze.

In order to evaluate the impact of the refreezing of melt ponds on the sea ice mass balance, we can estimate the difference in basal growth over the Arctic in the presence of ponds.

When a melt pond of 0.4 m is present on top of 1 m of ice the basal growth after 60 days is 0.02 m, while in the same amount of time a slab of ice would grow by 0.24 m.

Varying the ice thickness at the bottom of the pond leads to the following results: when the ice thickness is halved compared to our standard run (0.5 m compared to 1 m), the ice grows by 53 cm in a no-pond case and 20 cm in when a pond is present, while for a 1.5 m slab of ice the ice growth is 11 cm compared to no ice growth when considering a refreezing pond. The effect of refreezing pond is therefore more important on thin ice, also because ice growth is faster for thin ice. This leads to the conclusion that this process will be increasingly important in the future considering that the Arctic sea ice cover is on average thinning.

With a typical sea ice area of about 5.5 million km^2 in September, a refreezing pond coverage of 20% [*Flocco et al*., 2012] and using our model estimate of a 22 cm reduction in basal growth when a trapped pond is present, we calculate that ignoring trapped ponds in the growth calculation gives a corresponding overestimate of ice growth of 265 km^3 in about 2 months. This is approximately 25% of the average sea ice volume change in the same period estimated by PIOMAS [*Zhang and Rothrock*, 2003]. Considering that basal sea ice growth is faster for thin ice and that melt ponds form preferentially on thin ice, with a pond area greater than 20%, our calculations are likely to be an underestimate. This leads us to conclude that refreezing of melt ponds should not be neglected in future melt pond parameterizations for sea ice climate models.

Acknowledgments
We would like to acknowledge the Natural Environmental Research Council for supporting this work. The ERA-Interim data are available for download from http://data-portal.ecmwf.int/.

References

Bailey, E., D. L. Feltham, and P. R. Sammonds (2010), A model for the consolidation of rafted sea ice, *J. Geophys. Res.*, *115*, C04015, doi: 10.1029/2008JC005103.

Bitz, C., and W. Lipscomb (1999), An energy-conserving thermodynamic model of sea ice, *J. Geophys. Res.*, *104*(C7), 15,669–15,677, doi: 10.1029/1999JC900100.

Bogorodskiy, P. V., and A. V. Marchenko (2014), Thermodynamic effects accompanying freezing of two water layers separated by a sea ice sheet, *Oceanology*, *54*, 152–159.

Bogorodskiy, P. V., A. V. Marchenko, and A. V. Pnyushkov (2006), Thermodynamics of freezing melt ponds, paper presented at the 18th IAHR International Symposium on Ice, Sapporo, Japan, 28 August–1 September.

Ebert, E. E., and J. A. Curry (1993), An intermediate one-dimensional thermodynamic sea ice model for investigating ice-atmosphere interactions, *J. Geophys. Res.*, *98*(C6), 10,085–10,109, doi:10.1029/93JC00656.

Feltham, D. (1998), *Fluid dynamics and thermodynamics of sea ice*, PhD thesis, Univ. of Cambridge, Cambridge, U. K.

Feltham, D. L., and M. G. Worster (2000), Similarity solution describing the melting of a mush, *J. Cryst. Growth*, *208*, 746–756.

Feltham, D. L., N. Untersteiner, J. S. Wettlaufer, and M. G. Worster (2006), Sea ice is a mushy layer, *Geophys. Res. Lett.*, *33*, L14501, doi: 10.1029/2006GL026290.

Flocco, D., and D. L. Feltham (2007), A continuum model of melt pond evolution on Arctic sea ice, *J. Geophys. Res.*, *112*, C08016, doi:10.1029/2006JC003836.
Flocco, D., D. L. Feltham, and A. K. Turner (2010), Incorporation of a physically based melt pond scheme into the sea ice component of a climate model, *J. Geophys. Res.*, *115*, C08012, doi:10.1029/2009JC005568.
Flocco, D., D. Schroeder, D. L. Feltham, and E. C. Hunke (2012), Impact of melt ponds on Arctic sea ice simulations from 1990 to 2007, *J. Geophys. Res.*, *117*, C09032, doi:10.1029/2012JC008195.
Hunke, E. C., W. H. Lipscomb, and A. K. Turner (2010), Sea ice models for climate study: Retrospective and new directions, *J. Glaciol.*, *56*, 1162–1172.
Kwok, R., G. F. Cunningham, M. Wensnahan, I. Rigor, H. J. Zwally, and D. Yi (2009), Thinning and volume loss of Arctic sea ice: 2003–2008, *J. Geophys. Res.*, *114*, C07005, doi:10.1029/2009JC005312.
Lüthje, M., D. L. Feltham, P. D. Taylor, and M. G. Worster (2006), Modeling the summertime evolution of sea-ice melt ponds, *J. Geophys. Res.*, *111*, C02001, doi:10.1029/2004JC002818.
Marchenko, A., P. V. Bogorodsky, V. V. Gorbatsky, A. P. Makshtas, and A. V. Pnyushkov (2009), Structure and physico mechanical properties of sea ice in the central arctic studied in the expedition Arctic-2007, paper presented at 20th International Conference on Port and Ocean Engineering Under Arctic Conditions, June 9–12, Luleå, Sweden.
Martin, S., and P. Kauffman (1974), The evolution of under-ice melt ponds, or double diffusion at the freezing point, *J. Fluid Mech.*, *64*, 507–528, doi:10.1017/S0022112074002527.
Maykut, G. A., and N. Untersteiner (1971), Some results from a time-dependent thermodynamic model of sea ice, *J. Geophys. Res.*, *76*(6), 1550–1575, doi:10.1029/JC076i006p01550.
Notz, D., and M. G. Worster (2008), In situ measurements of the evolution of young sea ice, *J. Geophys. Res.*, *113*, C03001, doi:10.1029/2007JC004333.
Notz, D., M. G. McPhee, M. G. Worster, G. A. Maykut, K. H. Schluünzen, and H. Eicken (2003), Impact of underwater-ice evolution on Arctic summer sea ice, *J. Geophys. Res.*, *108*(C7), 3223, doi:10.1029/2001JC001173.
Perovich, D. K. (1990), Theoretical estimates of light reflection and transmission by spatially complex and temporally varying sea ice covers, *J. Geophys. Res.*, *95*(C6), 9557–9567.
Perovich, D. K., T. C. Grenfell, B. Light, B. C. Elder, J. Harbeck, C. Polashenski, W. B. Tucker III, and C. Stelmach (2009), Transpolar observations of the morphological properties of Arctic sea ice, *J. Geophys. Res.*, *114*, C00A04, doi:10.1029/2008JC004892.
Sakazume, S., and N. Seki (1978), Thermal properties of ice and snow at low temperature region, *Bull. JSME*, *44*(382), 2059–2069.
Schröder, D., D. L. Feltham, D. Flocco, and M. Tsamados (2014), September Arctic sea-ice minimum predicted by spring melt-pond fraction, *Nat. Clim. Change*, *4*, 353–357, doi:10.1038/NCLIMATE2203.
Schwerdtfeger, P. (1963), The thermal properties of sea ice, *J. Glaciol.*, *4*(36), 789–807.
Scott, F., and D. L. Feltham (2010), A model of the three-dimensional evolution of Arctic melt ponds on first-year and multiyear sea ice, *J. Geophys. Res.*, *115*, C12064, doi:10.1029/2010JC006156.
Skyllingstad, E. D., C. A. Paulson, and D. K. Perovich (2009), Simulation of melt pond evolution on level ice, *J. Geophys. Res.*, *114*, C12019, doi:10.1029/2009JC005363.
Taylor, P. D., and D. L. Feltham (2004), A model of melt pond evolution on sea ice, *J. Geophys. Res.*, *109*, C12007, doi:10.1029/2004JC002361.
Timco, G. W., and R. M. W. Frederking (1996), A review of sea ice density, *Cold Reg. Sci. Technol.*, *24*, 1–6, doi:10.1016/0165-232X(95)00007-X.
Weeks, W. F., and S. F. Ackley (1986), The growth, structure and properties of sea ice, in *The Geophysics of Sea Ice, NATO ASI Ser. B*, vol. 146, edited by N. Untersteiner, pp. 9–164, Martinus Nijhoff, Dordrecht, Netherlands.
Wells, A. J., J. S. Wettlaufer, and S. A. Orszag (2011), Brine fluxes from growing sea ice, *Geophys. Res. Lett.*, *38*, L04501, doi:10.1029/2010GL046288.
Zhang, J., and D. A. Rothrock (2003), Modeling global sea ice with a thickness and enthalpy distribution model in generalized curvilinear coordinates, *Mon. Weather Rev.*, *131*(5), 681–697.